Optimal 1D Trajectory Design for UAV-Enabled Multiuser Wireless Power Transfer

Yulin Hu, *Senior Member, IEEE,* Xiaopeng Yuan, Jie Xu, *Member, IEEE,* and Anke Schmeink, *Senior Member, IEEE*

Abstract

In this paper, we study an unmanned aerial vehicle (UAV)-enabled wireless power transfer network, where a UAV flies at a constant altitude in the sky to provide wireless energy supply for a set of ground nodes with a linear topology. Our objective is to maximize the minimum received energy among all ground nodes by optimizing the UAV's one-dimensional (1D) trajectory, subject to the maximum UAV flying speed constraint. Different from previous works that only provided heuristic and locally optimal solutions, this paper is the first time to present the globally optimal 1D UAV trajectory solution to the considered min-energy maximization problem. Towards this end, we first show that for any given speed-constrained UAV trajectory, we can always construct a maximum-speed trajectory and a speed-free trajectory, such that their combination can achieve the same received energy at all these ground nodes. Next, we transform the UAV-speed-constrained trajectory design problem into an equivalent UAV-speed-free problem, which is then optimally solved via the Lagrange dual method. The optimal 1D UAV trajectory solution follows the so-called successive hover-and-fly structure, i.e., the UAV successively hovers at a finite number of hovering points each for an optimized hovering duration, and flies among these hovering points at the maximum speed. Building upon the optimal UAV trajectory structure, we further present a low-complexity UAV trajectory design by first transforming the original problem into an equivalent non-convex problem with only the UAV hovering locations and durations as optimization variables, and then updating the trajectory via the successive convex approximation technique. Our analysis shows that the low-complexity design is guaranteed to converge to a suboptimal solution at a significantly lower complexity irrespective of the geographical network size. Numerical results show that the proposed low-complexity design actually achieves the same performance as the proposed optimal solution, and both of them outperform the benchmark algorithms in prior works under different scenarios.

Index Terms

Unmanned aerial vehicle, wireless power transfer, energy fairness, trajectory design, successive hover-and-fly.

I. Introduction

Unmanned aerial vehicles (UAVs) have found abundant applications in, e.g., cargo delivery, aerial inspection and surveillance, due to the relatively high payload and long endurance. In recent years, UAV-enabled wireless applications have attracted increasing attentions, as UAVs can be used for the quick deployment of on-demand wireless systems. Thanks to the presence of line-of-sight (LoS) aerial-to-ground (A2G) wireless links between UAVs and ground devices, UAV-enabled wireless networks are likely to have better system performance than conventional terrestrial wireless networks [1]. In general, there are two types of UAV-enabled wireless applications, namely, wireless communication and wireless power transfer (WPT), respectively. On one hand, UAVs can be utilized as mobile base stations (BSs) or relays to improve the coverage [2]–[6] and data-rate throughput [7]–[15] performance for wireless communication. On the other hand, UAVs can also be used as mobile energy transmitters (ETs) that fly in the sky to broadcast radio frequency (RF) signals to wirelessly charge low-power ground nodes (such as sensors and

This work was supported in part by the DFG research grant SCHM 2643/17, the National Natural Science Foundation of China (Project No. 61871137) and the open research fund of National Mobile Communications Research Laboratory, Southeast University (Project No. 2019D08).

Y. Hu, X. Yuan, and A. Schmeink are with ISEK Research Group, RWTH Aachen University, D-52074 Aachen, Germany (email: {hu, xiaopeng.yuan, schmeink}@ti.rwth-aachen.de).

J. Xu is with the School of Information Engineering, Guangdong University of Technology, Guangzhou 510006, China, and also with the National Mobile Communications Research Laboratory, Southeast University, Nanjing 211189, China (e-mail: jiexu@gdut.edu.cn). J. Xu is the corresponding author.

Internet-of-thing (IoT) devices) [16], [17]. Furthermore, UAV-enabled wireless powered communication networks [22]–[24] and wireless powered edge computing (see, e.g., [18]) have been studied in [15] and [19], respectively.

Due to the fully controllable mobility, UAVs provide new degrees of freedom in improving the wireless performance via optimizing UAVs' quasi-stationary deployment locations or time-varying locations over time (a.k.a. trajectories) [3]. For instance, the prior works [4]–[6], [9], [13] considered UAV-enabled cellular BSs, where the UAV's deployment locations are optimized to provide the maximum coverage for ground users [4]–[6], [9], and to enhance the performance of cell-edge users via data offloading [13]. In addition, in UAV-enabled mobile relaying systems, the UAV trajectory is jointly designed with the wireless resource allocation, so as to improve the throughput [10], [11] or enhance the energy efficiency [12].

On the other hand, UAV-enabled WPT has recently emerged as a promising solution to prolong the lifetime of low-power sensors and IoT devices, by using UAVs as mobile ETs to power these devices [15]–[17], [19]. In particular, by considering the UAV flying at a fixed altitude, the works [16], [17] optimized the one-dimensional (1D) or two-dimensional (2D) UAV trajectory to maximize the energy transfer performance for a UAV-enabled WPT network, subject to maximum UAV speed constraints. In a two-user scenario in a linear topology, the authors in [16] optimized the 1D UAV trajectory to characterize the Pareto boundary of the achievable energy region by the two users. This result is then extended to the general multiuser scenario in a 2D topology in [17], where the 2D UAV trajectory is optimized to maximize the minimum received energy among these users. The essential idea of the UAV trajectory design in [16], [17] is proceeded as follows. First, a relaxed problem is considered which ignores the UAV speed constraints, based on which it is shown that the optimal UAV trajectory solution to this relaxed problem follows a *multi-location-hovering* structure, where the UAV hovers at a finite number of locations with optimized hovering durations. Then, a heuristic *successive hover-and-fly* (SHF) trajectory is proposed for the general problem with the maximum UAV speed constraints considered, in which the UAV successively hovers over these locations, and then flies among them at the maximum speed. Next, the *successive convex approximation (SCA)* technique is further performed to refine the UAV trajectory, by quantizing the continuous UAV trajectory into a finite number of way points. It is worth noting that for the general case with the UAV maximum speed constraint considered, the heuristic SHF trajectory can only obtain generally suboptimal solutions, while the SCP-based trajectory design can only ensure the local optimality when the quantization size becomes extremely small. Nevertheless, such an accurate quantization will lead to extremely high computation complexity. Furthermore, in [16], [17] the structure of the optimal UAV trajectory solution still remains unknown, even for the basic case with two users. These issues[1] thus motivate us to characterize the optimal UAV trajectory structure and to design high-quality UAV trajectories at low complexity in this paper.

In this paper, we consider a simplified UAV-enabled WPT network with a linear topology, where $K > 1$ ground nodes are deployed in a straight line. To charge these nodes in an efficient and fair manner, we aim at maximizing the minimal received energy among all nodes via designing the UAV's 1D trajectory (or equivalently the velocity) for WPT, while the UAV mobility is subject to maximum speed constraints. The results of this work are summarized as follows.

- Different from previous works that only provided heuristic and locally optimal solutions, for the first time, we present the globally optimal 1D UAV trajectory solution to the considered WPT problem. Towards this end, we first show that for any given speed-constrained UAV trajectory, we can always construct a maximum-speed trajectory and a speed-free trajectory, such that their combination can

[1]It should be pointed out that there have been other prior works investigating UAV trajectory design for communication systems, e.g., in mobile edge networks [13] and cellular networks [7]. These designs generally obtained locally optimal or sub-optimal trajectory solutions. More recently, for a cellular-connected UAV network with pre-determined initial location and final location as well as minimum received signal-to-noise ratio (SNR) constraints, the authors in [20], [21] provided a flexible trade-off in the trajectory design between complexity and performance. The proposed trajectory design is able to approach the optimal solution with an arbitrarily small performance gap with polynomial complexity. For more general UAV-connected communication systems without specific distance/SNR constraints and with the initial location and final location to be optimized, how to reveal insightful structures and obtain optimal UAV trajectories are open questions that remain unaddressed.

achieve the same received energy at all these ground nodes. Next, we transform the original UAV-speed-constrained trajectory design problem into an equivalent UAV-speed-free problem, which is then optimally solved via the Lagrange dual method. It is proved that the optimal 1D UAV trajectory solution follows an interesting SHF structure, i.e., the UAV successively hovers at a finite number of hovering points each for an optimized hovering duration, and flies among these hovering points at the maximum speed. Moreover, we analyze the number of hovering points at the optimal trajectories. It is proved that there exists at least one optimal trajectory with the number of hovering points no larger than $K+2$.

- In addition to the optimal solution, an efficient and low-complexity UAV trajectory design is proposed. First, based on the proved structure of the optimal trajectory, we transform the original optimization problem as an equivalent non-convex problem with only the UAV hovering locations and durations as optimization variables. Then, we update the trajectory in an iterative manner by using the SCA technique. In each iteration, we approximate the non-convex problem into a convex one, and subsequently refine the trajectory towards a high-quality solution.
- Next, we analyze the complexities of the proposed optimal and suboptimal trajectory solutions in comparison to benchmark solutions in existing studies (e.g., the heuristic SHF and the SCP-based trajectory designs in [17]). In particular, it is shown that the computational complexity of our suboptimal design is constant irrespective of the geographical network size, which is advantageous over the optimal design in practical implementation. Via numerical results, we show that the proposed low-complexity design actually achieves the same performance as the proposed optimal solution, and both of them outperform the benchmark algorithms in prior works under different scenarios.

It is worth emphasizing that the obtained optimal SHF solution in this paper is in sharp contrast to the heuristic SHF design in [17], as the obtained UAV hovering locations and durations take into account the received energy during the UAV flying, while those in [17] ignore such impacts. Therefore, the proposed design achieves the optimal performance and outperforms the heuristic design in [17], as will be validated in our numerical results.

The remainder of this paper is organized as follows. We introduce the system model and formulate the min-energy maximization problem in Section II. In Section III, we characterize the optimal trajectory solution to the problem. Building upon the characterization, we propose an optimal trajectory design and a low-complexity trajectory design in Section IV. Section V analyzes the complexity level of our proposed designs versus other benchmark schemes. Finally, we provide simulation results in Section VI and conclude this work in Section VII.

II. System Model and Problem Formulation

In this paper, we consider a UAV-enabled multiuser WPT system with a linear topology as shown in Fig. 1, where a UAV flies at a fixed altitude $H>0$ to wirelessly charge a set $\mathcal{K}=\{1,\cdots,K\}$ of K ground nodes (such as IoT devices and sensors) that are located in a straight line, e.g., ground nodes are deployed within a limited distance interval along with a river, road or tunnel. We denote the horizontal location of

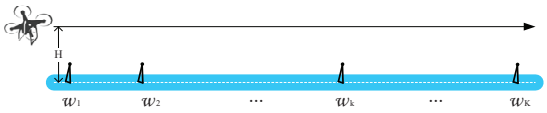

Fig. 1. Illustration of the UAV-enabled WPT network with a linear topology.

node $k\in\mathcal{K}$ as w_k. We assume that $w_1\le\cdots\le w_K$ without loss of generality. To efficiently charge all nodes, we focus on a finite UAV charging period $\mathcal{T}\overset{\Delta}{=}[0,T]$ with duration $T>0$. The UAV's time-varying horizontal location is denoted by $x(t)$ at time instant $t\in\mathcal{T}$. In addition, the UAV is subject to a maximal flying speed V. Hence, we have $|\dot{x}(t)|\le V, \forall t\in\mathcal{T}$, where $\dot{x}(t)$ denotes the first derivative of $x(t)$.

In practice, the wireless channels between the UAV and ground nodes are LoS-dominant, and therefore, we adopt the free-space path loss model as normally used in the UAV-enabled wireless communication and

WPT literature [10]. At time t, the channel power gain from the UAV to ground node $k \in \mathcal{K}$ is denoted as $h_k(x(t)) = \frac{\beta_0}{(x(t)-w_k)^2+H^2}$, where the distance between the UAV and ground node k is $\sqrt{(x(t)-w_k)^2+H^2}$ and β_0 is the channel power gain at a reference distance of unit meter. Hence, the received RF power by ground node k at time $t \in \mathcal{T}$ is

$$Q_k\left(x(t)\right) = \frac{\beta_0 P}{\left(x(t)-w_k\right)^2 + H^2}, \tag{1}$$

where P denotes the constant transmit power of the UAV. Notice that in practice, the received RF signal should be converted into a direct current (DC) signal to charge the rechargeable battery at each ground node, and the RF-to-DC conversion is in general a non-linear process [29]. In order to focus our study on the wireless transmission, we use the received RF power as the performance metric by ignoring the non-linear RF-to-DC conversion process, as in [16], [17].

Due to the broadcast nature of the wireless transmission, all ground nodes can simultaneously receive wireless power during the whole charging period $\mathcal{T}$. As a result, the total energy received by ground node $k \in \mathcal{K}$ is given by

$$E_k(\{x(t)\}) = \int_0^T Q_k\left(x\left(t\right)\right) dt. \tag{2}$$

Our objective is to design the UAV trajectory to maximize the minimal received energy among all the K nodes during the charging period T. In particular, it is assumed that the UAV is able to be freely deployed with both initial and final locations to be optimized. The problem of our interest is formulated as

$$\begin{aligned} (\mathrm{OP}): \max_{\{x(t)\}} \quad & \min_{k\in\mathcal{K}} \int_0^T Q_k(x(t))dt \\ \text{s.t.} \quad & |\dot{x}(t)| \le V, \forall t \in \mathcal{T}. \end{aligned} \tag{3}$$

By introducing an auxiliary variable E, the original problem (OP) is equivalently reformulated as

$$\begin{aligned} (\mathrm{P1}): \max_{\{x(t)\},E} \quad & E \\ \text{s.t.} \quad & \int_0^T Q_k(x(t))dt \ge E, \forall k \in \mathcal{K}, \\ & |\dot{x}(t)| \le V, \forall t \in \mathcal{T}. \end{aligned} \tag{4}$$

Notice that both the original problem (OP) and the reformulated problem (P1) are non-convex, due to the fact that the objective function in (OP) is non-concave, and constraint $\int_0^T Q_k(x(t))dt \ge E$ in (P1) is non-convex, respectively. Furthermore, both problems consist of an infinite number of variables $\{x(t)\}$ over continuous time. Therefore, how to find the optimal solution to the min-energy maximization problem is generally a very difficult task.

Note that in the prior work [17], the authors have proposed two designs, namely the heuristic SHF and the SCP-based trajectory solutions, which can also be used to solve (OP) and (P1) sub-optimally. However, as we discussed in Section I, the heuristic SHF trajectory solution is suboptimal, while the performance of the SCP-based trajectory can only ensure the local optimality even the quantization becomes extremely accurate. Moreover, the practical performance of the SCP-based trajectory depends on the quantization accuracy, and the implementation complexity is high especially when the quantization accuracy increases. It is still unknown how to obtain the optimal and well-structured 1D UAV trajectory solution to the min-energy maximization problem with maximum speed constraints.

III. Characterization of the Optimal Trajectory Solution to Problem (P1)

In this section, we characterize the optimal trajectory solution to problem (OP) or (P1). We show that it has an interesting SHF structure, in which the UAV hovers among a number of locations and then flies

among them at the maximum speed. This can significantly simplify the derivation of problem (P1), as will be shown in Section IV.

First, notice that there always exists a uni-directional trajectory[2] that is optimal for (P1), i.e., $x(t_1) \leq x(t_2), \forall t_1, t_2 \in \mathcal{T}, t_1 < t_2$. Therefore, in this paper we focus on the uni-directional trajectory without loss of optimality. Next, to characterize the structure of the optimal trajectory solution to problem (P1), we consider problem (P1) under a given pair of initial and final locations $x_{\rm I}$ and $x_{\rm F}$, i.e., $x(0) = x_{\rm I}$ and $x(T) = x_{\rm F}$. This sub-problem is given by

$$\begin{aligned} (\text{P1.1}): \max_{\{x(t)\}, E} \quad & E \\ \text{s.t.} \quad & \int_0^T Q_k(x(t))dt \geq E, \forall k \in \mathcal{K} \\ & |\dot{x}(t)| \leq V, \forall t \in \mathcal{T} \\ & x_{\rm I} \leq x(t) \leq x_{\rm F}, \forall t \in \mathcal{T}. \end{aligned} \tag{5}$$

Note that as the solution to (P1) is a special case (with optimal initial and final locations) of the solution to (P1.1), the structure of the optimal trajectory solution to (P1.1) holds also for the optimal trajectory solution to (P1).

In the following, we first show that any speed-constrained trajectory to problem (P1.1) is mathematically equivalent to the combination of a maximum-speed trajectory and a speed-free trajectory, and then provide the optimal solution to problem (P1.1) under any given pair of $x_{\rm I}$ and $x_{\rm F}$ via the Lagrange dual method. Accordingly, the structure of the optimal trajectory solution to problem (P1) will be characterized.

A. Problem Reformulation via Constructing Equivalent Max-Speed and Speed-Free Trajectories

We start with the following lemma to show that we can construct two trajectories for any unidirectional trajectory $\{x(t)\}$ satisfying the maximum speed constraint V.

Lemma 1. *For any duration-T unidirectional trajectory $\{x(t)\}$ satisfying the maximum speed constraint V with given initial position $x(0) = x_{\rm I}$ and final position $x(T) = x_{\rm F}$, we can always find two UAV trajectories $\{\bar{x}(t)\}$ and $\{\hat{x}(t)\}$ to jointly achieve the same WPT performance. In particular, $\{\bar{x}(t)\}$ is the max-speed flying with $\bar{x}(t) = x_{\rm I} + Vt, \forall t \in (0, \bar{T}]$, where $\bar{T} = (x_{\rm F} - x_{\rm I})/V$. In addition, $\{\hat{x}(t)\}$ has a time duration $\hat{T} = T - (x_{\rm F} - x_{\rm I})/V$ without any UAV speed constraints (speed-free). In other words, the following equality holds for any ground nodes.*

$$\begin{aligned} &\int_0^T Q_k\left(x\left(t\right)\right) dt \\ &\quad = \int_0^{\bar{T}} Q_k\left(\bar{x}\left(t\right)\right) dt + \int_0^{\hat{T}} Q_k\left(\hat{x}\left(t\right)\right) dt, \forall k \in \mathcal{K}. \end{aligned} \tag{6}$$

Proof. The proof is provided in Appendix A. □

Note that for the maximum-speed flying trajectory $\{\bar{x}(t)\}$ from $x_{\rm I}$ to $x_{\rm F}$, the trajectory is fixed, i.e., the UAV flies from $x_{\rm I}$ to $x_{\rm F}$ at the maximal speed V. In particular, for trajectory $\{\bar{x}(t)\}$, the received energy

[2]Assume that there exists an optimal trajectory $\{x_S(t)\}$ with path S, which is not uni-directional, i.e., the UAV flies forward and backward. Under $\{x_S(t)\}$, the UAV flies multiple times over each location on the (or a part of the) path S. Then, we can calculate the cumulative flying/hovering time duration of the UAV over each location on the path S. We can always find an alternative uni-directional UAV trajectory with the same path S to achieve the same WPT performance as $\{x_S(t)\}$, by letting the UAV fly with a relatively lower speed such that the flying/hovering time duration of the UAV over each location on S is the same as the cumulative flying/hovering time duration of the UAV over each location under $\{x_S(t)\}$. Hence, without loss of generality, there always exists a uni-directional trajectory solution being optimal to (P1).

by ground node $k \in \mathcal{K}$ is

$$\begin{aligned}\bar{E}_k &= \int_0^{\bar{T}} Q_k(\bar{x}\,(t))\,dt = \int_0^{\bar{T}} Q_k\left(x_{\mathrm{I}} + Vt\right)dt \\ &= \frac{\beta_0 P}{VH}\arctan(\frac{x_{\mathrm{F}}-w_k}{H}) - \frac{\beta_0 P}{VH}\arctan(\frac{x_{\mathrm{I}}-w_k}{H}).\end{aligned} \tag{7}$$

Based on Lemma 1, (P1.1) is equivalently reformulated as

$$\begin{aligned}(\mathrm{P2}):\ \max_{\{\hat{x}(t)\},E}\quad & E \\ \text{s.t.}\quad & \int_0^{\hat{T}} Q_k(\hat{x}(t))dt + \bar{E}_k \geq E,\ \forall k \in \mathcal{K} \\ & x_{\mathrm{I}} \leq \hat{x}(t) \leq x_{\mathrm{F}}, \forall t \in \hat{\mathcal{T}},\end{aligned} \tag{8}$$

where $\hat{\mathcal{T}} = [0, \hat{T}]$ and $\bar{E}_k$ is a constant defined in (7).

All problems (P1), (P1.1) and (P2) are non-convex but satisfy the so-called time-sharing condition from [30]. Hence, strong duality holds between each problem and its Lagrange dual problem. However, note that the constraint $|\dot{x}(t)| \leq V, \forall t \in \mathcal{T}$, in problem (P1) and problem (P1.1) is a time-continuous constraint, which cannot be decomposed over time. In other words, the dual Lagrange function of either problem (P1) and problem (P1.1) has an infinite number of Lagrange multipliers, which makes the problems non-tractable. On the other hand, as not having such constraints with location variables coupling over time, problem (P2) can be efficiently solved via the Lagrange dual method [31] with decomposition, which is actually the key motivation of reformulating problem (P1.1) to problem (P2).

B. Optimal Solution to Problem (P2)

Denote the Lagrange multipliers for the k-th constraint in (8) by $\lambda_k \geq 0, k \in \mathcal{K}$. The partial Lagrangian of (P2) is

$$\begin{aligned}&\mathcal{L}_2\left(\{\hat{x}(t)\}, E, \{\lambda_k\}\right) \\ &= E + \sum_{k\in\mathcal{K}} \lambda_k \left(\int_0^{\hat{T}} Q_k(\hat{x}(t))dt + \bar{E}_k - E \right) \\ &= (1 - \sum_{k\in\mathcal{K}} \lambda_k)E + \sum_{k\in\mathcal{K}} \lambda_k \bar{E}_k + \int_0^{\hat{T}} \sum_{k\in\mathcal{K}} \lambda_k Q_k(\hat{x}(t))dt.\end{aligned} \tag{9}$$

Immediately, we have the corresponding dual function as

$$\begin{aligned}f_2\left(\{\lambda_k\}\right) \quad = \quad & \max_{\{\hat{x}(t)\},E} \mathcal{L}_2\left(\{\hat{x}(t)\}, E, \{\lambda_k\}\right) \\ & \text{s.t.} \quad x_{\mathrm{I}} \leq \hat{x}(t) \leq x_{\mathrm{F}}, \forall t \in \hat{\mathcal{T}}.\end{aligned} \tag{10}$$

Clearly, the condition $1 - \sum_{k\in\mathcal{K}} \lambda_k = 0$ must be satisfied to guarantee that the function $f_2(\{\lambda_k\})$ is upper-bounded from above, i.e., $f_2(\{\lambda_k\}) < \infty$. Otherwise, if $1 - \sum_{k\in\mathcal{K}} \lambda_k < 0$ (or $1 - \sum_{k\in\mathcal{K}} \lambda_k > 0$), we have $f_2\left(\{\lambda_k\}\right) \to \infty$ by setting $E \to -\infty$ (or $E \to \infty$). Then, the dual problem of (P2) is

$$\begin{aligned}(\mathrm{DP2}):\ \min_{\{\lambda_k\}}\quad & f_2(\{\lambda_k\}) \\ \text{s.t.}\quad & 1 - \sum\nolimits_{k\in\mathcal{K}} \lambda_k = 0, \quad \lambda_k \geq 0, \forall k \in \mathcal{K}.\end{aligned} \tag{11}$$

According to the solution to problem (P3.1) in [17], the dual function can be obtained by solving the

following problem

$$\begin{aligned} \max_{\hat{x}} \quad & F(\hat{x}) \triangleq \sum\nolimits_{k\in\mathcal{K}} \lambda_k Q_k(\hat{x}) \\ \text{s.t.} \quad & x_{\rm I} \le \hat{x} \le x_{\rm F}. \end{aligned} \tag{12}$$

Moreover, we can obtain the extreme points of $F(\hat{x})$ by letting its first order derivative be zero, i.e., $F'(\hat{x}) = \sum_{k\in\mathcal{K}} \lambda_k \frac{-2(\hat{x}-w_k)\beta_0 P}{((\hat{x}-w_k)^2+H^2)^2} = 0$, which equals to solve

$$\sum_{k=1}^{K} \Big\{ -2(\hat{x}-w_k)\beta_0 P\lambda_k \cdot \prod_{i\neq k}^{i\in\mathcal{K}} \left((\hat{x}-w_i)^2 + H^2\right)^2 \Big\} = 0. \tag{13}$$

In other words, the extreme points of $F(\hat{x})$ can be obtained by solving (13). By comparing the objective values in (12) at the extreme points versus those at the boundary points $x_{\rm I}$ and $x_{\rm F}$, the optimal hovering points $\hat{x}_1^*, \hat{x}_2^*, ..., \hat{x}_N^*$ are obtained, where N denotes the number of optimal solutions which achieves the same objective value. Accordingly, the dual function $f(\{\lambda_k\})$ is obtained.

With $f(\{\lambda_k\})$ obtained, the dual problem (DP2) can be solved via the ellipsoid method, and therefore, the solution $\{\lambda_k^*\}$ is obtained. Based on $\{\lambda_k^*\}$, we can reconstruct the primal optimal solution to (P2) by solving the time-sharing problem for allocating the total duration T over the N hovering points, for which the optimization problem is formulated as the following linear program (LP):

$$\begin{aligned} \max_{\{\hat{\tau}_i\ge 0\},E} \quad & E \\ \text{s.t.} \quad & \sum\nolimits_{i=1}^{N} \hat{\tau}_i Q_k(\hat{x}_i) + \bar{E}_k \ge E, \forall k \in \mathcal{K} \\ & \sum\nolimits_{i=1}^{N} \hat{\tau}_i = \hat{T}. \end{aligned} \tag{14}$$

By solving this LP problem via standard interior point method, we obtain the optimal hovering durations $\hat{\tau}_1^*, \hat{\tau}_2^*, ..., \hat{\tau}_N^*$ corresponding to the N hovering points. Therefore, (P2) is optimally solved under the given $x_{\rm I}$ and $x_{\rm F}$. In summary, the optimal solution to (P2) is described by the optimal hovering points and hovering durations

$$\hat{x}^*(t) = \hat{x}_i^*, \text{ if } t \in \Big[\sum\nolimits_{j=1}^{i} \hat{\tau}_j^* - \hat{\tau}_i^*, \ \sum\nolimits_{j=1}^{i} \hat{\tau}_j^* \Big], \ i = 1, \cdots, N. \tag{15}$$

It is observed that the optimal solution to (P2) has a multi-location-hovering structure. Note that the left side of (13) is a $4K-3$ order polynomial of $\hat{x}$, i.e., $F(\hat{x})$ has at most $4K-3$ extrema and therefore at most $2K-1$ maximum points as potential hovering points. In addition, the two boundary points $x_{\rm I}$ and $x_{\rm F}$ are also potential hovering points. Hence, there are a maximum number of $2K+1$ hovering locations in the optimal solution to (P2). Fortunately, we can further show that there exists an optimal multi-location-hovering solution to (P2) with only K hovering locations required as follows.

Lemma 2. *There exists one optimal multi-location-hovering solution to problem (P2) with the number of hovering points being no more than K, i.e., $N \le K$.*

Proof. The proof is provided in Appendix B. □

C. Optimal Solution to Problem (P1.1)

In Section III-B, we have shown that for given $x_{\rm I}$ and $x_{\rm F}$, the global optimal trajectory problem (P2) can be obtained. Suppose that the corresponding optimal solution to problem (P2) $\hat{x}(t)$ with optimal hovering points $\hat{x}_1^*, \hat{x}_2^*, ..., \hat{x}_N^*$ and the corresponding optimal hovering durations. $\hat{\tau}_1^*, \hat{\tau}_2^*, ..., \hat{\tau}_N^*$. According to Lemma 1, we can express the optimal solution to (P1.1) by combining $\hat{x}(t)$ with $\bar{x}(t) = x_{\rm I} + Vt, \forall t \in (0, \bar{T}]$, i.e., letting the UAV fly at the maximal speed from $x_{\rm I}$ to $x_{\rm F}$ while stopping/hovering at the N

$$x^*(t)=\begin{cases}\hat{x}_i^*, & \text{if } \sum\limits_{j=1}^{i}\hat{\tau}_j^*-\hat{\tau}_i^*+\frac{x_i^*-x_0^*}{V}\le t\le \sum\limits_{j=1}^{i}\hat{\tau}_j^*+\frac{x_i^*-x_1^*}{V},\ 1\le i\le N+1,\\ x_0^*+V(t-\sum\limits_{j=1}^{i}\hat{\tau}_j^*), & \text{if } \sum\limits_{j=1}^{i}\hat{\tau}_j^*+\frac{x_i^*-x_0^*}{V}\le t\le \sum\limits_{j=1}^{i}\hat{\tau}_j^*+\frac{x_{i+1}^*-x_0^*}{V},\ 1\le i\le N.\end{cases} \tag{16}$$

hovering points (in between) with the corresponding optimal hovering durations. By defining $x_0^*=x_{\rm I}^*$, $x_{N+1}^*=x_{\rm F}^*$ and $\hat{\tau}_0^*=\hat{\tau}_{N+1}^*=0$, we have the optimal solution $\{x^*(t)\}$ to problem (P1.1), given in (16).

D. Structure of Optimal Trajectory Solution to Problem (P1)

In this subsection, we describe the structure of this optimal trajectory solution to (P1) in the following proposition.

Proposition 1. *The optimal trajectory solution to problem (P1.1) or problem (P1) follows the SHF structure, i.e., there exists a number of N hovering locations at the optimal trajectory, such that the UAV always flies at the maximum speed from one hovering location to another, and then hovers at that location for a certain time duration. Furthermore, there always exists an optimal trajectory with no more than $K+2$ hovering locations , i.e., $N\le K+2$.*

Proof. Combining Lemmas 1 and 2, this proposition is verified directly for problem (P1.1). In particular, recall that the minimum number of hovering points in $\hat{x}(t)$ is upper-bounded by K, where these hovering points are not necessarily including $x_{\rm I}$ and $x_{\rm F}$, since in $\hat{x}(t)$ the UAV does not have a speed constraint to really start and end at $x_{\rm I}$ and $x_{\rm F}$. Then, in $x(t)$ the UAV flies from $x_{\rm I}$ to $x_{\rm F}$ with a limited speed, these two points are possible to be hovering points of $x(t)$.

In addition, note that the globally optimal trajectory to problem (P1) is obtained by applying a 2D exhaustive search over the possible pair of $x_{\rm I}$ and $x_{\rm F}$, i.e., the optimal solution to problem (P1) is the best one in the solutions of all the problems (P1.1) with different $x_{\rm I}$ and $x_{\rm F}$. Hence, as the optimal solution to any problem (P1.1) has an SHF structure, the globally optimal trajectory to problem (P1) also has such a structure. Therefore, Proposition 1 is finally proved. □

IV. Optimal and Low-Complexity Trajectory Solutions to Problem (P1)

Following the provided characterization in Section III on the optimal trajectory, in this section we propose the optimal solution and a low-complexity suboptimal solution to (P1).

A. Optimal Solution to Problem (P1)

In Section III-C, we have shown that the global optimal trajectory to problem (P1.1) is obtained, i.e., we have optimally solved problem (P1) under given $x_{\rm I}$ and $x_{\rm F}$. Hence, by applying a 2D exhaustive search over the possible pair of $x_{\rm I}$ and $x_{\rm F}$ together with solving (P1.1) under each $x_{\rm I}$ and $x_{\rm F}$, the global optimally trajectory solution to (P1) is finally obtained.

It is clear there is no benefit if the UAV hovers at a position out of the region of ground nodes[3]. Hence, the feasible set of $x_{\rm I}$ is $[w_1,w_K]$ while the corresponding feasible set of $x_{\rm F}$ is $[x_{\rm I},w_K]$. To apply the exhaustive search on $x_{\rm I}$ or $x_{\rm F}$ within its continuous feasible set, we introduce $d_{\min}$ as the resolution in distance. Note that we have $d_{\min}$ should be small and let $\frac{w_K-w_1}{d_{\min}}$ be an integer. Hence, feasible locations of $x_{\rm I}$ and the corresponding $x_{\rm F}$ become $\{w_1,w_1+d_{\min},w_1+2d_{\min},\cdots,w_K\}$ and $\{x_{\rm I},x_{\rm I}+d_{\min},x_{\rm I}+2d_{\min},\cdots,w_K\}$, respectively. The flow chart of the optimal solution to (P1) is shown in Fig. 2.

[3]For any trajectory $\{x_1(t)\}$ with the initial location $x_{\rm I}<w_1$ and the flying time t_0 from $x_{\rm I}$ to w_1, there always exists another trajectory $\{x_2(t)\}$ that achieves a higher WPT performance than $\{x_1(t)\}$, where $\{x_2(t)\}$ has an initial location exactly at w_1 with hovering time t_0 (at w_1) while the rest part (after w_1) is the same as $\{x_1(t)\}$.

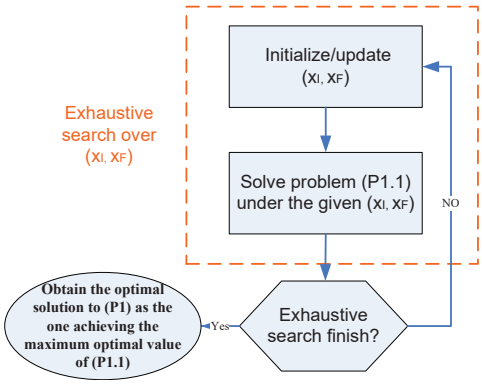

Fig. 2. Flow chart for deriving the optimal solution to problem (P1).

$$x(t)=\begin{cases} x_i, & \text{if } \sum_{j=1}^{i}\tau_j-\tau_i+\frac{x_i-x_1}{V}\le t\le \sum_{j=1}^{i}\tau_j+\frac{x_i-x_1}{V},\ 1\le i\le K+2,\\ x_1+V(t-\sum_{j=1}^{i}\tau_j), & \text{if } \sum_{j=1}^{i}\tau_j+\frac{x_i-x_1}{V}\le t\le \sum_{j=1}^{i}\tau_j+\frac{x_{i+1}-x_1}{V},\ 1\le i\le K+1. \end{cases} \tag{17}$$

B. An Efficient Low-Complexity Trajectory Design to (P1)

In this subsection, we propose an efficient trajectory approach based on the optimal SHF structure as shown in Proposition 1. According to this structure, in order solve problem (P1), we actually only need to find the $K+2$ hovering points $\{x_1,...,x_{K+2}\}$ (at maximum) satisfying $w_1\le x_1\le x_2\le\cdots\le x_{K+2}\le w_K$ and the corresponding hovering durations $\{\tau_1,...,\tau_{K+2}\}$. Notice that these $K+2$ hovering points already include the initial and finial locations, which are also potential optimal hovering points to problem (P1). If the optimal trajectory solution only has less than $K+2$ hovering points, this corresponds to the case when we have zero hovering durations for certain locations. Therefore, this model (with $K+2$ hovering points and their hovering durations) is general enough to characterize the optimal trajectory. Following the structure of the optimal solution given in (16), the trajectory with $K+2$ hovering points is expressed in (17) on the next page.

By substituting (17) into (7), we have

$$\begin{aligned} E_k(\mathbf{x},\mathbf{t}) =& E_{k,\text{Hov}}(\mathbf{x},\mathbf{t})+E_{k,\text{Fly}}(x_1,x_{K+2})\\ =&\sum_{i=1}^{K+2}E_{k,i,\text{Hov}}(x_i,\tau_i)+E_{k,\text{Fly}}(x_1,x_{K+2})\\ =&\sum_{i=1}^{K+2}\frac{\beta_0P\tau_i}{(x_i-w_k)^2+H^2}+\frac{\beta_0P}{VH}\arctan(\frac{x_{K+2}-w_k}{H})\\ &-\frac{\beta_0P}{VH}\arctan(\frac{x_1-w_k}{H}), \end{aligned} \tag{18}$$

where $E_{k,i,\text{Hov}}(x_i,\tau_i)=\frac{\beta_0P\tau_i}{(x_i-w_k)^2+H^2}$ denotes the received energy at node k during UAV hovering at the hovering point i and $E_{k,\text{Hov}}(\mathbf{x},\mathbf{t})=\sum_{i=1}^{K+2}E_{k,i,\text{Hov}}(x_i,\tau_i)$ denotes the sum of received energy at node k when UAV hovering at all $K+2$ hovering points. In addition, $E_{k,\text{Fly}}(x_1,x_{K+2})=\frac{\beta_0P}{VH}\arctan(\frac{x_{K+2}-w_k}{H})-\frac{\beta_0P}{VH}\arctan(\frac{x_1-w_k}{H})$ denotes the received energy at node k during the UAV flying. Therefore, problem (P1)

is equivalently transformed as

$$\begin{aligned}(\mathrm{P3}): \max_{\mathbf{x},\mathbf{t},E} \quad & E \\ \text{s.t.} \quad & E_k(\mathbf{x},\mathbf{t}) \geq E, \forall\, k \in \mathcal{K}\,, \\ & \sum\nolimits_{i=1}^{K+2} \tau_i + \frac{x_{K+2}-x_1}{V} = T\,, \\ & w_1 \leq x_1 \leq x_2 \leq \cdots \leq x_{K+2} \leq w_K\,, \\ & t_i \geq 0, \forall i \in \{1,2,\cdots,K+2\},\end{aligned} \tag{19}$$

where the second constraint $\sum_{i=1}^{K+2} \tau_i + \frac{x_{K+2}-x_1}{V} = T$ ensures that the whole charging duration T must be fully utilized.

Although problem (P3) is non-convex as the first constraint is not convex, we present an efficient solution by applying the SCA technique. It should be pointed out that the proposed approach is different from the conventional alternating optimization, which has been widely applied in UAV trajectory design to handle non-convex trajectory optimization problems, but is not applicable to problem (P3). In particular, if we apply the alternating optimization, problem (P3) can be solved by alternatively optimizing $\mathbf{t}$ and $\mathbf{x}$, i.e., the problem of t is linear and the problem of x can be approximated to a convex problem via the Taylor expansions. However, we can easily find in the alternating optimization that $\sum_{i=1}^{K+2} \tau_i$ is constant for given $\mathbf{t}$ and that $\sum_{i=1}^{K+2} \tau_i$ is also constant for given $\mathbf{x}$ according to the constraint $\sum_{i=1}^{K+2} \tau_i + \frac{x_N-x_1}{V} = T$. In other words, the sum of the hovering durations (and therefore the total flying time corresponding to the distance between x_1 and x_{K+2}) never changes under the alternating optimization. This leads to an unchanged objective value and thus results in a highly suboptimal solution when the initial point is badly chosen.

To efficiently solve problem (P3), in the following two subsections, we first present a new convex approximation for the problem at any given local point $(\mathbf{x}^{(r)}, \mathbf{t}^{(r)})$ in the r-th iteration, and then propose an efficient iterative algorithm.

1) Convex Approximation: In this subsection, we design a new convex approximation for problem (P3), where the aim is to provide a concave function for each iteration, namely function $E_k^{(r)}$ for the r-th iteration, such that $E_k \geq E_k^{(r)}$ and the equality holds at the local point $(\mathbf{x}^{(r)}, \mathbf{t}^{(r)})$ in the iteration. According to (18), the energy E_k received by ground node k are from two parts. In the following, we provide concave functions to approximate these two parts respectively.

We start with the part of energy received when UAV is hovering while distinguishing $\tau_i^{(r)} > 0$ and $\tau_i^{(r)} = 0$:

- Case $\tau_i^{(r)} > 0$: We obtain the approximation $f_{i,k}^{(r)}(x_i, \tau_i)$ in the following way:
  Note that function $\frac{1}{(x_i-w_k)^2+H^2}$ is convex in $(x_i-w_k)^2$. According to the first order condition, it holds for the two points $(x_i-w_k)^2$ and $(x_i^{(r)}-w_k)^2$ that

$$\begin{aligned}E_{k,i,\mathrm{Hov}}(x_i,\tau_i) &= \frac{\beta_0 P \tau_i}{(x_i-w_k)^2+H^2} \\ &\geq -A_{i,k}^{(r)}\Big((x_i-w_k)^2-(x_i^{(r)}-w_k)^2\Big)\,\tau_i + B_{i,k}^{(r)}\tau_i,\end{aligned} \tag{20}$$

  where $A_{i,k}^{(r)} = \frac{\beta_0 P}{((x_i^{(r)}-w_k)^2+H^2)^2}$ and $B_{i,k}^{(r)} = \frac{\beta_0 P}{(x_i^{(r)}-w_k)^2+H^2}$. Clearly, the equality of (20) holds when $x_i = x_i^{(r)}$. Moreover, by introducing two positive constants $C_{i,k}^{(r)} > 0$, $D_{i,k}^{(r)} > 0$, we have the inequality shown in (21) on the top of next page. The inequality in (21) follows the inequality of arithmetic and geometric means [25], i.e., $ab \leq \frac{1}{2}a^2 + \frac{1}{2}b^2$ where the quality holds when $a = b$. In addition, $F_{i,k}^{(r)} = \frac{\tau_i^{(r)}+D_{i,k}^{(r)}}{(x_i^{(r)}-w_k)^2+C_{i,k}^{(r)}}$ is introduced to guarantee the equality of (21) at $x_i = x_i^{(r)}$. Combining the derivations from (20) to (21), we can have following (lower-bounded) approximation of $E_{k,i,\mathrm{Hov}}$, which is given in (22) on the

$$(x_i-w_k)^2\tau_i = \underline{\Big((x_i-w_k)^2+C_{i,k}^{(r)}\Big)\Big(\tau_i+D_{i,k}^{(r)}\Big)} - C_{i,k}^{(r)}\tau_i - D_{i,k}^{(r)}(x_i-w_k)^2 - C_{i,k}^{(r)}D_{i,k}^{(r)}$$
$$\leq \underline{\frac{F_{i,k}^{(r)}}{2}\Big((x_i-w_k)^2+C_{i,k}^{(r)}\Big)^2 + \frac{1}{2F_{i,k}^{(r)}}\Big(\tau_i+D_{i,k}^{(r)}\Big)^2} - C_{i,k}^{(r)}\tau_i - D_{i,k}^{(r)}(x_i-w_k)^2 - C_{i,k}^{(r)}D_{i,k}^{(r)}. \tag{21}$$

$$\begin{aligned} E_{k,i,\mathrm{Hov}}(x_i,\tau_i) &\geq -A_{i,k}^{(r)}((x_i-w_k)^2-(x_i^{(r)}-w_k)^2)\tau_i + B_{i,k}^{(r)}\tau_i \\ &\geq -\frac{A_{i,k}^{(r)}F_{i,k}^{(r)}}{2}\Big((x_i-w_k)^2+C_{i,k}^{(r)}\Big)^2 - \frac{A_{i,k}^{(r)}}{2F_{i,k}^{(r)}}(\tau_i+D_{i,k}^{(r)})^2 + A_{i,k}^{(r)}(x_i^{(r)}-w_k)^2\tau_i \\ &\quad + B_{i,k}^{(r)}\tau_i + A_{i,k}^{(r)}C_{i,k}^{(r)}\tau_i + A_{i,k}^{(r)}D_{i,k}^{(r)}(x_i-w_k)^2 + A_{i,k}^{(r)}C_{i,k}^{(r)}D_{i,k}^{(r)} \\ &\triangleq f_{i,k}^{(r)}(x_i,\tau_i), \end{aligned} \tag{22}$$

top of next page, while $f_{i,k}^{(r)}(x_i,\tau_i) = E_{k,i,\mathrm{Hov}}$ holds at point $x_i = x_i^{(r)}$, as the two inequalities have been shown to be inequalities under the case. Moreover, to guarantee the concavity of $f_{i,k}^{(r)}(x_i,\tau_i)$, $F_{i,k}^{(r)}$ is required to be limited by $F_{i,k}^{(r)} \in \Big(0, \frac{\tau_i^{(r)}}{(x_i^{(r)}-w_k)^2}\Big]$. In other words, the choices of $C_{i,k}^{(r)}$, $D_{i,k}^{(r)}$ should stratify $0 < \frac{\tau_i^{(r)}+D_{i,k}^{(r)}}{(x_i^{(r)}-w_k)^2+C_{i,k}^{(r)}} \leq \frac{\tau_i^{(r)}}{(x_i^{(r)}-w_k)^2}$.

- Case $\tau_i^{(r)} = 0$, $f_{i,k}^{(r)}(x_i,\tau_i)$ is given by

$$\begin{aligned} f_{i,k}^{(r)}(x_i,\tau_i) &\triangleq \frac{\beta_0 P\tau_i}{\max\big\{(w_1-1w_k)^2,(w_K-w_k)^2\big\}+H^2} \\ &\leq \frac{\beta_0 P\tau_i}{(x_i-w_k)^2+H^2}. \end{aligned} \tag{23}$$

On the one hand, the inequality holds, as $\max\big\{(w_1-w_k)^2,(w_K-w_k)^2\big\} \geq (x_i-w_k)^2$. On the other hand, the equality also holds at point $x_i = x_i^{(r)}$, as $\tau_i = 0$ makes both sides of the inequality be zeros. Moreover, $f_{i,k}^{(r)}(x_i,\tau_i)$ is linear and therefore concave.

Next, we discuss the approximation for $E_{k,\mathrm{Fly}} = \frac{\beta_0 P}{VH}\arctan(\frac{x_{K+2}-w_k}{H}) - \frac{\beta_0 P}{VH}\arctan(\frac{x_1-w_k}{H})$, which is the difference/gap between two $\arctan$ functions. Although the convexity/concavity of the $\arctan$ function is clear, i.e., $\arctan(\mu)$ is convex when $\mu > 0$ and concave when $\mu < 0$, it is still difficult to provide a concave function to approximate for $E_{k,\mathrm{Fly}}$ due to the fact that (as $\min\{\mathbf{w}\} \leq x_1 \leq x_2 \leq \cdots \leq x_{K+2} \leq \max\{\mathbf{w}\}$) $x_{K+2}-w_k$ and x_1-w_k are possible to be either both positive or both negative or one positive and one negative.

In this work, we obtain the approximation $g_k^{(r)}(x_1,x_N)$ in the following way: i. We first reformulate $E_{k,\mathrm{Fly}}$ to be the sum of two $\arctan$ functions, i.e., $E_{k,\mathrm{Fly}}(x_1,x_N) = \frac{\beta_0 P}{VH}\arctan(\frac{x_{K+2}-w_k}{H}) + \frac{\beta_0 P}{VH}\arctan(\frac{w_k-x_1}{H})$. ii. Then, we approximate each $\arctan$ function to a concave quadratic function, while this quadratic function is the lower bound of the original $\arctan$ function and the two functions have the same value case $(x_1^{(r)}, x_{K+2}^{(r)}) = (x_1, x_{K+2})$. As a result, the sum of two concave functions is also concave and is the lower bound of $E_{k,\mathrm{Fly}}$ while having the same value as $E_{k,\mathrm{Fly}}$ case $(x_1^{(r)}, x_{K+2}^{(r)}) = (x_1, x_{K+2})$. Following the above methodology, we provide in Lemma 3 a process to obtain a lower bound concave quadratic function for function $\arctan(z)$, while the two functions have the same value at a local point $z = z_0$.

Lemma 3. *Given an upper-bounded variable $z \in (-\infty, Z]$, and a local point z_0, $z_0 \leq Z$, there exists*

such a, b, c guaranteeing the following two conditions:

$$\arctan(z) \geq -az^2 + bz + c, \forall x \in (-\infty, Z], a \geq 0, \tag{24}$$

$$\arctan(z_0) = -az_0^2 + bz_0 + c. \tag{25}$$

An example solution of a, b, c satisfying (24) *and* (25)*, can be obtained in the following*

i. *Define*

$$a = \max\left\{0, -\frac{\arctan(Z) - \arctan(z_0) + \frac{z_0 - Z}{z_0^2+1}}{(Z - z_0)^2}\right\}. \tag{26}$$

ii. *If $a > \frac{1}{2(Z-z_0)(z_0^2+1)}$, we redefine a as the positive root of the following equation*

$$16(z_0^2+1)^2a^2 - 8z_0(z_0^2+1)a - 1 = 0. \tag{27}$$

iii. *Based on a, we define*

$$b = \frac{1}{z_0^2+1} + 2az_0, \tag{28}$$

$$c = \arctan(z_0) + az_0^2 - bz_0. \tag{29}$$

Proof. The proof of Lemma 3 is provided in Appendix B. □

According to the example solution in Lemma 3, for a local hovering point $\mathbf{x}^{(r)}$ in the r-th iteration, we can find corresponding $(a_{K+2,k}^{(r)}, b_{K+2,k}^{(r)}, c_{K+2,k}^{(r)})$ and $(a_{1,k}^{(r)}, b_{1,k}^{(r)}, c_{1,k}^{(r)})$ to approximate $\arctan(\frac{x_{K+2}-w_k}{H})$ and $\arctan(\frac{w_k-x_1}{H})$ by $-a_{K+2,k}^{(r)}(\frac{x_{K+2}-w_k}{H})^2 + b_{K+2,k}^{(r)}\frac{x_{K+2}-w_k}{H} + c_{K+2,k}^{(r)}$ and $-a_{1,k}^{(r)}(\frac{w_k-x_1}{H})^2 + b_{1,k}^{(r)}\frac{w_k-x_1}{H} + c_{1,k}^{(r)}$, respectively. In particular, according to Lemma 3, the $(a_{K+2,k}^{(r)}, b_{K+2,k}^{(r)}, c_{K+2,k}^{(r)})$ and $(a_{1,k}^{(r)}, b_{1,k}^{(r)}, c_{1,k}^{(r)})$, which are depending on $x_{K+2}^{(r)}$ and $x_1^{(r)}$, definitely guarantee $\arctan(\frac{x_{K+2}-w_k}{H}) = -a_{K+2,k}^{(r)}(\frac{x_{K+2}-w_k}{H})^2 + b_{K+2,k}^{(r)}\frac{x_{K+2}-w_k}{H} + c_{K+2,k}^{(r)}$ at $x_{K+2}^{(r)} = x_{K+2}$ and $\arctan(\frac{w_k-x_1}{H}) = -a_{1,k}^{(r)}(\frac{w_k-x_1}{H})^2 + b_{1,k}^{(r)}\frac{w_k-x_1}{H} + c_{1,k}^{(r)}$ at $x_1^{(r)} = x_1$.

Define by $g_k^{(r)}(x_1, x_N)$ the approximation of $E_{k,\mathrm{Fly}}$ in the r-th iteration. Hence, for any feasible point/trajectory $\mathbf{x}$ in problem (P3), $g_k^{(r)}(x_1, x_N)$ is given by

$$\begin{aligned} g_k^{(r)}(x_1, x_{K+2}) &\triangleq \frac{\beta_0 P}{VH}\Big(-a_{K+2,k}^{(r)}(\frac{x_{K+2}-w_k}{H})^2 + b_{K+2,k}^{(r)}\frac{x_{K+2}-w_k}{H} \\ &\qquad + c_{K+2,k}^{(r)} - a_{1,k}^{(r)}(\frac{w_k-x_1}{H})^2 + b_{1,k}^{(r)}\frac{w_k-x_1}{H} + c_{1,k}^{(r)}\Big) \\ &\leq \frac{\beta_0 P}{VH}\arctan(\frac{x_{K+2}-w_k}{H}) + \frac{\beta_0 P}{VH}\arctan(\frac{w_k-x_1}{H}) \\ &= \frac{\beta_0 P}{VH}\arctan(\frac{x_{K+2}-w_k}{H}) - \frac{\beta_0 P}{VH}\arctan(\frac{x_1-w_k}{H}) \\ &= E_{k,\mathrm{Fly}}(x_1, x_{K+2}), \end{aligned} \tag{30}$$

while $g_k^{(r)}(x_1, x_N) = E_{k,\mathrm{Fly}}(x_1, x_N)$ holds in the case of $(x_1^{(r)}, x_{K+2}^{(r)}) = (x_1, x_{K+2})$.

So far, we have obtained the (lower-bounded) approximations, i.e., $f_{i,k}^{(r)}(x_i, t_i)$ and $g_k^{(r)}(x_1, x_{K+2})$, for $E_{k,i,\mathrm{Hov}}(x_i, t_i)$ and $E_{k,\mathrm{Fly}}(x_1, x_{K+2})$, respectively. As a result, for any feasible point/trajectory $\mathbf{x}$ of problem (P3) we have the combined approximation $E_k^{(r)}(\mathbf{x}, \mathbf{t})$

$$\begin{aligned} E_k^{(r)}(\mathbf{x}, \mathbf{t}) &= \sum\nolimits_{i=1}^{N} f_{i,k}^{(r)}(x_i, t_i) + g_k^{(r)}(x_1, x_{K+2}) \\ &\leq E_k(\mathbf{x}, \mathbf{t}). \end{aligned} \tag{31}$$

Based on the above designs, $f_{i,k}^{(r)}(x_i, t_i) = E_{k,i,\mathrm{Hov}}(x_i, t_i)$, $i = 1, \cdots, K+2$ and $g_k^{(r)}(x_1, x_N)$ are concave.

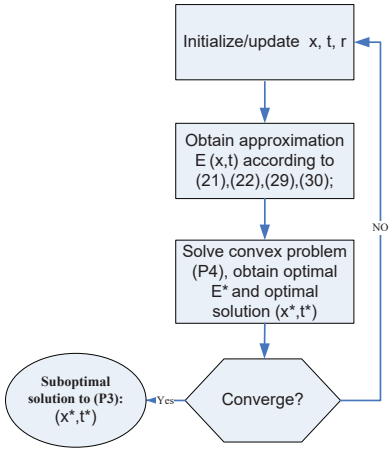

Fig. 3. Flow chart of optimally solving problem (P3).

In addition, it has been shown that $\forall i = 1, \cdots, K+2$, $f_{i,k}^{(r)}(x_i, t_i) = E_{k,i,\text{Hov}}(x_i, t_i)$ holds when $x_i^{(r)} = x_i$ and that $g_k^{(r)}(x_1, x_N) = E_{k,\text{Fly}}(x_1, x_N)$ holds when $(x_1^{(r)}, x_{K+2}^{(r)}) = (x_1, x_{K+2})$. Hence, we can conclude that $E_k^{(r)}(\mathbf{x}, \mathbf{t})$ is concave and that the equality in (31) holds at $(\mathbf{x}^{(r)}, \mathbf{t}^{(r)})$.

2) Iterative Algorithm: Based on the above convex approximation, in the following we propose an iterative solution for (P3). In the initialization step, we set a feasible local point $(\mathbf{x}^0, \mathbf{t}^0)$ by uniformly scattering points on a line segment in interval $[w_1, w_k]$ and uniformly allocating hovering time at each hovering point. Clearly, the line segments lie in the interval $[w_1, w_k]$ and the sum length of the segments is less than VT.

After the initialization step, the algorithm starts the iteration. In the r-th iteration, we first derive a convex approximation of problem (P3) at a local point $(\mathbf{x}^{(r)}, \mathbf{t}^{(r)})$. Then, following the convex approximation design provided in the previous subsection, we have an approximated problem provided in (P4)

$$\begin{aligned} (\text{P4}): \max_{\mathbf{x},\mathbf{t},E} \quad & E \\ s.t. \quad & E_k^{(r)}(\mathbf{x}, \mathbf{t}) \geq E, \forall k \in \{1, 2, \cdots, K\}, \\ & \sum_{i=1}^{N} \tau_i + \frac{x_{K+2} - x_1}{V} = T, \\ & t_i \geq 0, \ \forall i \in \{1, 2, \cdots, K+2\}. \end{aligned} \tag{32}$$

TABLE I
COMPLEXITY LEVEL COMPARISON

Algorithm	Complexity level
Proposed optimal SHF	$\mathcal{O}\left(\max(K, \frac{D}{d_{\min}})K^3(\frac{D}{d_{\min}})^2 \log(\frac{1}{\epsilon})\right)$
Proposed low-complexity SHF	$\mathcal{O}\left(\varphi K^4 \log(\frac{1}{\epsilon})\right)$
Heuristic SHF[17]	$\mathcal{O}\left(\max(K, \frac{D}{d_{\min}})K^3 \log(\frac{1}{\epsilon})\right)$
SCP with time quantization[17]	$\mathcal{O}\left(\max(K, \frac{D}{d_{\min}})K^3 \log(\frac{1}{\epsilon})\right)+\mathcal{O}\left(\varphi(\frac{T}{t_{\min}})^3 \max(\frac{T}{t_{\min}}, K) \log(\frac{1}{\epsilon})\right)$

Note that $E_k^{(r)}(\mathbf{x}, \mathbf{t})$ is concave. Problem (P4) is a convex and can be solved efficiently. Then, the solution to problem (P4) is used as the local point in the next iteration.

According to the above analysis, the flow chart of this iterative algorithm is provided in Fig 3.

V. COMPLEXITY LEVEL ANALYSIS

In this section, we discuss the complexity of the proposed trajectory designs, i.e., **proposed optimal SHF** in Section III and **proposed low-complexity SHF** in Section IV-B, in comparison to two recent

benchmark solutions in [17], i.e., **heuristic SHF** and **SCP with time quantization**, as we discussed after (P1) in Section II.

A comment characteristic of these four designs is that the trajectories are obtained in an iterative manner for minimizing convex functions. Note that there are many iterative methods can be applied (in these designs), which definitely results in different complexities. To provide a fair complexity comparison, we assume that all the three trajectory designs use the same quantization size for iteration and the iterations stop at the same error threshold $\epsilon > 0$. In particular, we assume that the ellipsoid method is applied for the iterations, motivated by the two characteristics of the ellipsoid method [26]: On the one hand, the ellipsoid method generates a sequence of ellipsoids whose volume uniformly decreases at each step, thus efficiently converging to a minimizer of a convex function after finite rounds of iterations. On the other hand, its complexity depends on the number of variables and the related calculation of the objective and constraint functions [27], which facilitates our complexity analysis. According to the complexity analysis in [27], when applying the ellipsoid method to solve a convex sub-problem with N variables, $\mathcal{O}(N^2\log(\frac{1}{\epsilon}))$ calls, namely iterations in the ellipsoid method for ellipsoid updates, are required, while in **each** call additional computational complexity is introduced due to the calculation of the objective and constraint functions. For the computational complexity in each call, we evaluate the floating point operations based on the operation analysis in [28].

The results of complexity comparison are provided in Table 1, where φ denotes the number of iterations of the two iterative algorithms till achieving the convergence, i.e., the error threshold ϵ is satisfied. Moreover, $d_{\min}$ represents the resolution in distance for the exhaustive search and $t_{\min}$ is the quantization size in the SCP with time quantization. In the proposed optimal SHF, there are in total $\mathcal{O}\big((\frac{D}{d_{\min}})^2\big)$ pairs of $(x_{\rm I}, x_{\rm F})$ in the exhaustive search. For each pair of $(x_{\rm I}, x_{\rm F})$, a dual problem with K variables (K Lagrange multipliers) is solved, corresponding to $\mathcal{O}\big(K^2\log(\frac{1}{\epsilon})\big)$ calls. In each call, complexities of $\mathcal{O}(K^2)$ and $\mathcal{O}(K\frac{D}{d_{\min}})$ are introduced respectively due to the ellipsoid updates [27] and solving (13) based on the analysis in [28]. Therefore, the complexity level of optimal SHF is given by $\mathcal{O}\left((\frac{D}{d_{\min}})^2\right)\cdot\mathcal{O}(K^2\log(\frac{1}{\epsilon}))\cdot\left(\mathcal{O}\left(K^2\right)+\mathcal{O}(K\frac{D}{d_{\min}})\right)=\mathcal{O}\left(\max(K,\frac{D}{d_{\min}})K^3(\frac{D}{d_{\min}})^2\log(\frac{1}{\epsilon})\right)$. For the proposed suboptimal design (low-complexity SHF), in each iteration of the algorithm, a convex problem with $2N$ variables is required to be solved, resulting in $\mathcal{O}\left((2N)^2\log(\frac{1}{\epsilon})\right)$ calls in the ellipsoid method. In each call, the complexities of ellipsoid updates and of the objective function calculation are respectively $\mathcal{O}((2N)^2)$ and $\mathcal{O}\left(KN\right)$. As the number of iterations of this iterative method is given by φ and the number of hovering points N is proved to be $N=K+2$, the complexity level of this design is given by $\varphi\mathcal{O}\left((2N)^2\log(\frac{1}{\epsilon})\right)\cdot(\mathcal{O}((2N)^2)+\mathcal{O}\left(KN\right))=\mathcal{O}\left(\varphi K^4\log(\frac{1}{\epsilon})\right)$. Next, the complexity of the heuristic SHF is the same as that of the Optimal SHF with a given $(x_{\rm I}, x_{\rm F})$ pair. Hence, the total complexity level of the heuristic SHF is given by $\mathcal{O}\left(\max(K,\frac{D}{d_{\min}})K^3\log(\frac{1}{\epsilon})\right)$. Finally, the SCP with time quantization is actually a further improvement based on the result of the heuristic SHF. Hence, the complexity of it is the sum of the heuristic SHF and the additional SCP process, where the SCP process has $\frac{T}{t_{\min}}$ variables, resulting in $\mathcal{O}\left(\varphi(\frac{T}{t_{\min}})^3\max(\frac{T}{t_{\min}},K)\log(\frac{1}{\epsilon})\right)$ level of complexity.

Clearly, to have an accurate trajectory solution, $d_{\min}$ and $t_{\min}$ are required to be sufficiently small, which lets $\frac{D}{d_{\min}}$ and $\frac{T}{t_{\min}}$ be significantly larger than the other terms in the complexity expressions of all solutions. In this case, the SCP with time quantization is expected to have the highest complexity, i.e., its complexity level has the order of $(\frac{T}{t_{\min}})^4$. In addition, the proposed optimal SHF and the heuristic SHF are also have high complexities, as their complexities are in the orders of $(\frac{D}{d_{\min}})^3$ and $\frac{D}{d_{\min}}$, respectively. Hence, the complexities of these three algorithms are decreasing in $d_{\min}$ and/or $t_{\min}$ and increasing in the geographical network size D. At the same time, the complexity level of the proposed low-complexity SHF is **not** influenced by the resolutions $d_{\min}$ and $t_{\min}$, i.e., it is not influenced by the geographical network size D with given resolutions. As a result, it is expected to introduce a significantly low complexity while providing an efficient WPT performance.

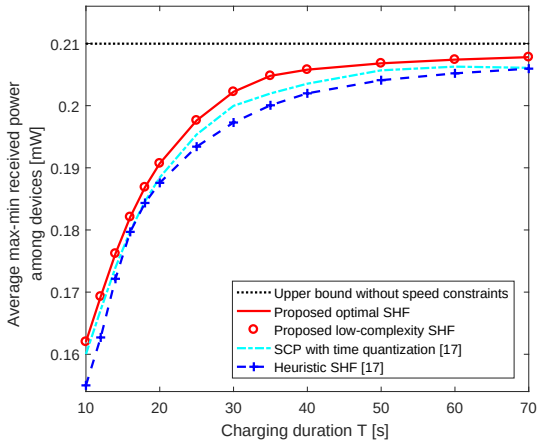

Fig. 4. Average WPT performance (over 20 realizations of random ground node topologies) versus the charging duration T.

VI. Numerical Results

In this section, we evaluate the proposed optimal SHF and the proposed low-complexity SHF, in comparison to the heuristic SHF [17] and the SCP with time quantization [17], following the complexity comparison in the previous section. To obtain the WPT performance, we randomly drop ground nodes to have 20 different topologies, and then apply these four algorithms at each topology, and finally average of the max-min received power among all ground nodes over these random realizations. In the simulation, we have the following default setups of parameters: $\beta_0 = -30\ dB$, $P = 40\ dBm$, $K = 5$, $N = K + 2$, $H = 5\ m$, $T = 20\ s$, $V = 1\ m/s$ and $D = 20\ m$. In addition, we set the quantization size of distance for the exhaustive search to $d_{\min} = 0.01\ m$ and set accordingly the time quantization size in the reference algorithm SCP with time quantization to $t_{\min} = d_{\min}/V$.

Fig. 4 shows the impact of the charging duration T on the WPT performance, where the upper bound of the ideal case with UAV speed constraint ignored is also provided. First, it is observed that, as the charging duration T increases, the performance of all the four algorithms increases towards the upper bound. In addition, owning to applying additional SCP process, the SCP with time quantization has a better performance than the heuristic SHF, which is consistent with the results in [17]. More importantly, both the proposed algorithms (optimal SHF and low-complexity SHF) outperform the two reference algorithms, in the whole charging duration regime. In particular, the proposed low-complexity SHF achieves a similar performance of the optimal SHF (although it has a significantly low complexity than the rest three algorithms), which confirms the performance advantages of this algorithm. It should be mentioned that in addition to Fig. 4 we have also done more simulations (not shown due to space limitation), where similar relationships among the algorithms are observed under scenarios with relatively short charging durations T.

Fig. 5 shows relationship between the WPT performance and UAV speed V. From the figure, we learn that under all algorithms, the max-min received power increases as the UAV speed V becomes larger. In addition, as the speed significantly increases, all the four designs are observed to approach the upper bound. Moreover, we observe again the performance advantage of the proposed algorithms in comparison to the two reference algorithms. We have also studied scenarios with relatively high maximal speeds V, similar results (not provided here due to space limitation) are also observed. Furthermore, recall that the heuristic SHF has two steps: first solving the relaxed problem assuming an infinite UAV speed and then based on it obtaining a new trajectory by using TSP or SCP to satisfy the speed constraint. In other words, there exists a certain performance loss of the heuristic SHF in comparison to the optimal trajectory solution. However, when the UAV speed becomes faster (more closer to the infinite speed), this performance loss is reduced. On the other hand, as shown in the figure, the proposed low-complexity SHF has almost the same performance as the proposed optimal solution. As a result, the performance

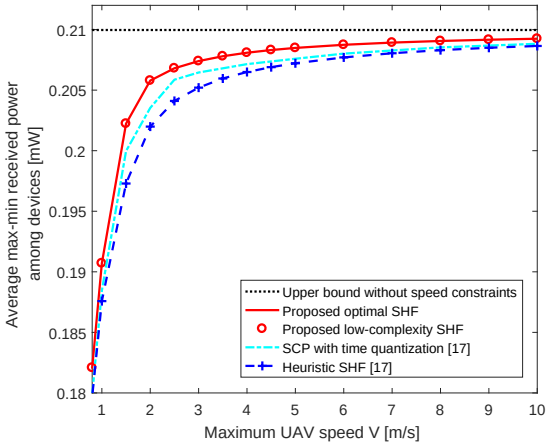

Fig. 5. Average WPT performance (over 20 realizations of random ground node topologies) versus the maximum UAV speed V.

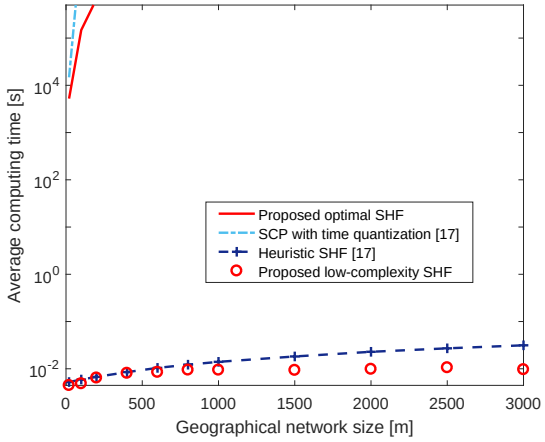

Fig. 6. The comparison in terms of computing time (over 20 realizations of random ground node topologies) with $d_{\min} = 0.01$ m for the proposed optimal SHF. For the SCP with time quantization, we set $t_{\min} = d_{\min}/V$, which decreases as V increases.

advantages of proposed algorithms are reduced, when the speed of the UAV becomes faster.

Next, we provide a complexity comparison in Fig. 6 among the four algorithms in terms of the average computing time. In the comparison, we scale the geographical network size D together with the UAV speed V while keeping $D/V = T$. By doing so, we can observe the impact of D on the complexities of these algorithms, while $D/V = T$ guarantees that the scenarios are meaningful, i.e., if the speed of UAV is too slow to fly over the network, there is no time for hovering and the system gains less from all trajectory design algorithms. It should be noticed that with a fixed resolution in distance or time, the computing time of the proposed optimal SHF and the SCP with time quantization are significantly long for a network with a relatively large geographical size. Due to time limitation, we only obtain partial results (in the cases with relatively short geographical network size) of the proposed optimal SHF and the SCP with time quantization. We observe that the proposed optimal SHF has relatively less complexity than the SCP with time quantization, which matches well with our analysis at the end of Section V. Recall that the complexities of the optimal SHF and the SCP with time quantization are in the orders of $(\frac{D}{d_{\min}})^3$ and $(\frac{T}{t_{\min}})^4$, respectively. Note that in the simulation of Fig. 6, both $\frac{D}{d_{\min}}$ and $\frac{T}{t_{\min}}$ are linearly increasing in D. Hence, the complexities of the optimal SHF and the SCP with time quantization generally increase polynomially in the order of $\frac{D}{d_{\min}} = \frac{T}{t_{\min}} = 100D$. Moreover, combining with results from Fig. 4 and Fig. 5, it is validated that the proposed optimal SHF provides a higher WPT performance than the SCP with time quantization while spending less complexity. Furthermore, the results clearly show the advantage of the proposed low-complexity SHF. In particular, the figure confirms our analytical results in Section V that the

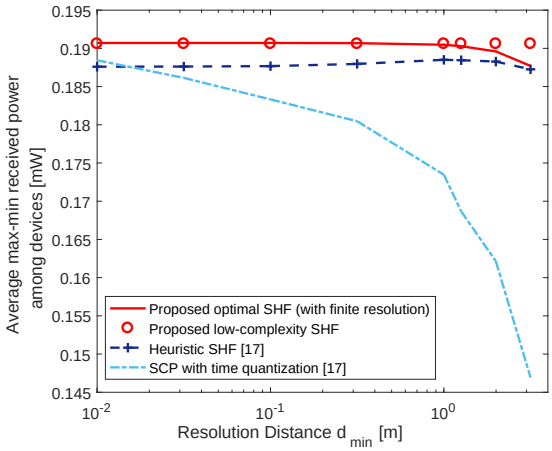

Fig. 7. The WPT performance comparison in terms of the resolution in exhaustive search. In the figure, we vary $d_{\min}$ directly while updating $t_{\min} = d_{\min}/V$ accordingly for the SCP with time quantization.

complexity level of the proposed low-complexity SHF is not influenced by the geographical network size. These results actually indicate the practical importance of the proposed structure of optimal trajectories as well as the proposed low-complexity SHF following the structure.

Note that the comparison in Fig. 6 is based on setups of resolutions $d_{\min}$ and $t_{\min}$ with relatively small value. We finally study in Fig. 7 how much these resolutions influence the performance of the four algorithms. It is observed from the figure that the impacts of resolutions on these algorithms are quite different. First of all, as expected, the proposed low-complexity SHF is not influenced by the resolution and it always provides an outstanding WPT performance.

Secondly, the SCP with time quantization significantly relies on the resolution, i.e., a relatively large value of $t_{\min}$ results in a poor performance. In particular, it provides a competitive performance (to other algorithms) only when spending significant complexity, i.e., $t_{\min} \leq 10^{-2}s$. Note that this algorithm actually approximates a flying trajectory in a time slot/resolution to a hovering point and treats the flying time in the time slot/resolution as the corresponding hovering time. For a given $t_{\min} > 0$, the real performance based on the SCP result is more likely to be lower than the ideal results (i.e., the optimum of the approximation) of the SCP process. This is actually the reason why the SCP with time quantization has a lower performance than the rest algorithms (including the heuristic SHF) when $t_{\min}$ is not significantly small. Finally, the performance of both the proposed optimal SHF and the heuristic SHF are not quite sensitive to $d_{\min}$, especially when $d_{\min}$ is not extremely large. The reason is as follows. In the heuristic SHF, the exhaustive search is applied for obtaining the hovering points. After that, the heuristic SHF further provides an hovering time allocation based on these points. Hence, the performance improvement of the hovering time allocation could migrate the impact of the inaccuracy of the hovering points. For an extreme example, the hovering time allocation process is possible to allocate zero time for a bad hovering point. On the other hand, it is surprising that the proposed optimal SHF provides an excellent performance even with a relatively large $d_{\min}$. Note that a relatively large $d_{\min}$ results in slightly inaccurate locations of $(x_{\mathrm{I}}, x_{\mathrm{F}})$. Hence, the proposed optimal SHF has actually been shown to be not sensitive in slight errors on $(x_{\mathrm{I}}, x_{\mathrm{F}})$, as for given $(x_{\mathrm{I}}, x_{\mathrm{F}})$ the algorithm will further adjust the optimal hovering points and optimal hovering durations, i.e., migrating the impact of the inaccuracy of $(x_{\mathrm{I}}, x_{\mathrm{F}})$.

VII. Conclusion

In this paper, we focus on a UAV-enabled WPT network with a linear topology. We studied the 1D UAV trajectory design problem with the objective of maximizing the minimal received power among all ground nodes, subject to the maximum UAV speed constraints. Different from previous works that only provided heuristic and locally optimal solutions, for the first time, we presented the globally optimal 1D UAV trajectory solution to the considered WPT problem in an SHF structure. Following the optimal SHF

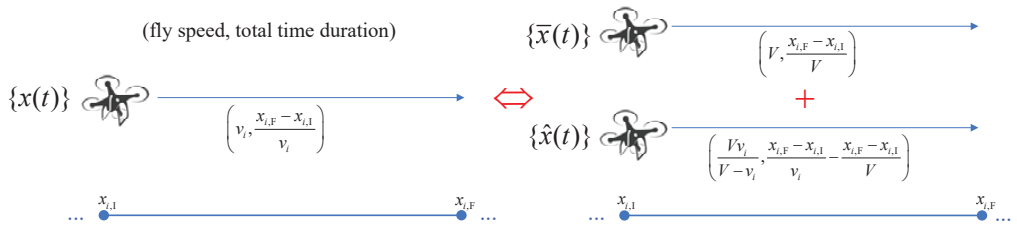

Fig. 8. Under Case 3, the WPT performance of $\{x(t)\}$ from $x_{\rm I}$ to $x_{\rm F}$ is equivalent to $\{\bar{x}(t)\}$ together with $\{\hat{x}(t)\}$.

$$\underbrace{\int_0^{\frac{x_{i,\rm F}-x_{i,\rm I}}{v_i}} \frac{\beta_0 P dt}{(x_{i,\rm I}+v_i t-w_k)^2+H^2}}_{\{x(t)\}} = \frac{v_i}{V}\int_0^{\frac{x_{i,\rm F}-x_{i,\rm I}}{v_i}} \frac{\beta_0 P dt}{(x_{i,\rm I}+v_i t-w_k)^2+H^2} + \frac{V-v_i}{V}\int_0^{\frac{x_{i,\rm F}-x_{i,\rm I}}{v_i}} \frac{\beta_0 P dt}{(x_{i,\rm I}+v_i t-w_k)^2+H^2}$$

$$\overset{\substack{v_i t = V t_1 \\ v_i t = \frac{V v_i}{V-v_i} t_2}}{=} \underbrace{\int_0^{\frac{x_{i,\rm F}-x_{i,\rm I}}{V}} \frac{\beta_0 P dt_1}{(x_{i,\rm I}+V t_1-w_k)^2+H^2}}_{\{\bar{x}(t)\}} + \underbrace{\int_0^{\frac{x_{i,\rm F}-x_{i,\rm I}}{v_i}-\frac{x_{i,\rm F}-x_{i,\rm I}}{V}} \frac{\beta_0 P dt_2}{(x_{i,\rm I}+\frac{V v_i}{V-v_i}t_2-w_k)^2+H^2}}_{\{\hat{x}(t)\}}. \tag{33}$$

structure, we proposed an efficient low-complexity trajectory design by using the SCA technique. It is shown via analysis and simulations that this proposed low-complexity design has a constant complexity irrespective of the geographical network size, i.e., thus making it quite promising for practical implementation. Numerical results confirm the performance advantage of the proposed optimal and low-complexity SHF trajectory designs, in comparison to benchmark schemes in the existing literature.

It is worth noting that our proposed trajectory design principles can be extended to UAV-enabled wireless communications with information broadcasting (see, e.g., [14]) and multicasting (see, e.g., [32]) with a 1D network topology, e.g., communication users are located in a line on the ground. It is expected that our proof technique can also be used to show that the optimal trajectory in such networks still follows the SHF structure. Accordingly, how to obtain the optimal hovering locations jointly with the wireless resource allocation is an interesting problem.

It is also worth noting that our proposed 1D trajectory design provides insights into the more general 2D/3D trajectory designs. For instance, it can be similarly shown that the UAV also follows the SHF trajectory structure. However, the maximum-speed flying path (curve) in 2D/3D scenarios becomes crucial for the performance optimization, i.e., the UAV flying path still needs to be optimized even hovering points are determined. How to design such path becomes an interesting issue that is non-trivial and left for our future work.

Appendix A
Proof of Lemma 1

This lemma can be proved by partitioning the whole time duration T into a sufficiently large number of time portions, each with a sufficiently small length such that during the portion the UAV speed is constant. Denote the length of i-th portion by $\tau_i, i = 1, \cdots, I$ and we have $\sum_{i=1,\cdots,I} \tau_i = T$. In addition, denote by v_i the speed of the UAV at the i-th portion, i.e., $0 \le v_i \le V$. Hence, there are three cases at each portion: Case 1. the UAV hovers at a given location, i.e., $v_i = 0$; Case 2. the UAV flies from $x_{i,\rm I}$ to $x_{i,\rm F}$ with speed $v_i = V$; Case 3. the UAV flies from $x_{i,\rm I}$ to $x_{i,\rm F}$ with speed $0 < v_i < V$.

In the following, we prove Lemma 1 by showing that within each time portion the UAV trajectory satisfying the maximum speed constraint is equivalent to two trajectories as defined in the lemma. The i-th portion of $\{x(t)\}$, the corresponding parts in $\{\bar{x}(t)\}$ and $\{\hat{x}(t)\}$ can be developed in the following way:

$$\sum_{j\neq i}\Big(\tau_j-\frac{\tau_i}{s_i}s_j+\frac{\tau_i}{M-1}(1-\sum_{j\neq i}(-\frac{s_j}{s_i}))\Big)\mathbf{u}_j \;=\; \sum_{j\neq i}\tau_j\mathbf{u}_j-\frac{\tau_i}{s_i}\sum_{j\neq i}s_j\mathbf{u}_j+\sum_{j\neq i}\Big(\frac{\tau_i}{M-1}(1+\sum_{j\neq i}\frac{s_j}{s_i})\Big)\mathbf{u}_j$$

$$\overset{s_i\mathbf{u}_i=-\sum_{j\neq i}s_j\mathbf{u}_j}{=}\sum_{m=1}^{M}t_m\mathbf{u}_m+\sum_{j\neq i}\Big(\frac{\tau_i}{M-1}(1+\sum_{j\neq i}\frac{s_j}{s_i})\Big)\mathbf{u}_j \;=\; (E_1,\cdots,E_K)^T+\sum_{j\neq i}\Big(\frac{\tau_i}{M-1}(1+\sum_{j\neq i}\frac{s_j}{s_i})\Big)\mathbf{u}_j \quad (34)$$

- Case 1: When the UAV is hovering in the portion, just let the $\{\hat{x}(t)\}$ have the same hovering point and the same hovering time τ_i.
- Case 2: When the UAV flies from $x_{i,\mathrm{I}}$ to $x_{i,\mathrm{F}}$ with the maximal speed, i.e., $v_i=V$, just let trajectory $\{\bar{x}(t)\}$ have the same trajectory as $\{x(t)\}$ in this portion. Hence, in Case 2 trajectory $\{\hat{x}(t)\}$ not covers the interval between $x_{i,\mathrm{I}}$ and $x_{i,\mathrm{F}}$. Hence, the trajectory (in terms of not time but topology) of $\{\hat{x}(t)\}$ is not continuous, i.e., there is not speed limit of the UAV in $\{\hat{x}(t)\}$.
- Case 3: In this case, the UAV flies from $x_{i,\mathrm{I}}$ to $x_{i,\mathrm{F}}$ with a speed lower than the maximal speed, i.e., $0<v_i<V$. The length of the portion is $\tau_i=\frac{x_{i,\mathrm{F}}-x_{i,\mathrm{I}}}{v_i}$.
  As shown in Fig. 8, we can let the UAV fly with the maximal speed in $\{\bar{x}(t)\}$ which has the time cost $\frac{x_{i,\mathrm{F}}-x_{i,\mathrm{I}}}{V}$. In addition, we let the UAV in $\{\hat{x}(t)\}$ use the remaining time, i.e., $\frac{x_{i,\mathrm{F}}-x_{i,\mathrm{I}}}{v_i}-\frac{x_{i,\mathrm{F}}-x_{i,\mathrm{I}}}{V}$, to fly from $x_{i,\mathrm{I}}$ to $x_{i,\mathrm{F}}$, while the corresponding speed can be calculated as $\frac{x_{i,\mathrm{F}}-x_{i,\mathrm{I}}}{\frac{x_{i,\mathrm{F}}-x_{i,\mathrm{I}}}{v_i}-\frac{x_{i,\mathrm{F}}-x_{i,\mathrm{I}}}{V}}=\frac{Vv_i}{V-v_i}$.
  Note that when v_i becomes significantly close to V and therefore the corresponding UAV speed in $\{\hat{x}(t)\}$ is possible to be sufficient large, which confirms again no speed limit for the UAV in $\{\hat{x}(t)\}$. It can be shown that in i-th portion the WPT performance of $\{x(t)\}$ and the sum WPT performance of $\{\bar{x}(t)\}$ and $\{\hat{x}(t)\}$ are the same $\forall k=1,\cdots,K$, given in (33).

So far, for each portion of $\{x(t)\}$, we can obtain the corresponding parts of $\{\bar{x}(t)\}$ and $\{\hat{x}(t)\}$ having the same WPT performance as the portion of $\{x(t)\}$. By repeating the above process for every portion of $\{x(t)\}$, $\{\bar{x}(t)\}$ and $\{\hat{x}(t)\}$ can be developed while satisfying Lemma 1.

APPENDIX B
PROOF OF LEMMA 2

We show that at most K hovering points can achieve the optimal performance. Assume there are M hovering points in an optimal trajectory without UAV speed limit. We denote these hovering points and corresponding non-zero hovering time by $x_1,\cdots,x_M$ and $\mathbf{t}=(\tau_1,\cdots,\tau_M)$. We define a charging matrix $\mathbf{U}=(u_{mk})_{M\times K}$, where $u_{mk}=Q_k(x_m)=\frac{\beta_0 P}{(x_m-w_k)^2+H^2}$ and $\mathbf{u}_m$ is the m-th row of matrix $\mathbf{U}$. Then, the received energy at devices can be obtained by $\sum_{m=1}^{M}\tau_m\mathbf{u}_m=(E_1,\cdots,E_K)^T$.

In the following, we prove $N\leq K$ holds (at least for one optimal trajectory) by showing: For an optimal trajectory with $M>\mathbf{rank}(\mathbf{U})$ hovering points, we can always find a trajectory that achieves the same WPT performance but with only $\mathbf{rank}(\mathbf{U})$ hovering points.

If $M>\mathrm{rank}(\mathbf{U})$, the rows of matrix $\mathbf{U}$ will be linearly dependent, i.e., there exists $s_m\neq 0, m=1,\cdots,M$ such that $\sum_{m=1}^{M}s_m\mathbf{u}_m=\mathbf{0}^{1\times K}$. Hence, we have the following lemma

Lemma 4. *For an optimal trajectory with $M>\mathbf{rank}(\mathbf{U})$ hovering points, $\sum_{m=1}^{M}s_m=0$ holds.*

Proof. This lemma is proved by contradiction while distinguish the following two cases:

Case 1: when $\sum_{m=1}^{M}s_m>0$, we let $i=\arg\min_{m,s_m>0}\frac{\tau_m}{s_m}$. Then, we delete the hovering point i and allocate the hovering time on remaining hovering points to obtain a better performance. The hovering time re-allocation is definited as

$$\begin{cases}\tau_j\longrightarrow\tau_j-\frac{\tau_i}{s_i}s_j+\frac{\tau_i}{M-1}(1-\sum_{j\neq i}(-\frac{s_j}{s_i})), & \text{when } j\neq i\,,\\ \tau_j\longrightarrow 0 & \text{when } j=i\end{cases}$$

Note that the total charging duration does not change, i.e.,

$$\sum_{j\neq i}\Big(\tau_j-\frac{\tau_i}{s_i}s_j+\frac{\tau_i}{M-1}(1-\sum_{j\neq i}(-\frac{s_j}{s_i}))\Big)=\sum_{j\neq i}\tau_j+\tau_i.$$

And $\tau_j-\frac{\tau_i}{s_i}s_j\geq 0$ holds due to $i=\arg\min_{m,s_m>0}\frac{\tau_m}{s_m}$, $1-\sum_{j\neq i}(-\frac{s_j}{s_i})>0$ holds due to $\sum_{m=1}^{M}s_m>0$ and $s_i>0$. Thus, the hovering time in new allocation is still larger than zero. For the new allocation, the received energy is given in (34). Note that in vector $\sum\limits_{j\neq i}\Big(\frac{\tau_i}{M-1}(1+\sum\limits_{j\neq i}\frac{s_j}{s_i})\Big)\mathbf{u}_j$ each element is positive, i.e., all devices receive more energy in the new allocation. Thus, $\sum_{m=1}^{M}s_m>0$ does not hold.

Case 2: when $\sum_{m=1}^{M}s_m<0$, we define $i=\arg\max\limits_{m,s_m<0}\frac{\tau_m}{s_m}$ and do the same allocation. In the same way as above, it can be proved that there is also an allocation scheme with a better performance.

Therefore, $\sum_{m=1}^{M}s_m=0$ holds in an optimal trajectory when $M>\mathbf{rank}(\mathbf{U})$. □

For an optimal trajectory S.1 with $M>\mathbf{rank}(\mathbf{U})$, the hovering point i can be determined according to $i=\arg\min\limits_{m}\frac{\tau_m}{|s_m|}$. Then, we can obtain a new trajectory S.2 by deleting this hovering point i and re-allocating its hovering time to the rest hovering points of S.1 following (B). According to (34), as $1+\sum_{j\neq i}\frac{s_j}{s_i}=0$, S.1 and S.2 have the same WPT performance, i.e., S.2 is also optimal. By iteratively applying this process of deleting hovering point and re-allocating hovering time, we finally obtain an optimal trajectory with only $\mathbf{rank}(\mathbf{U})$ hovering points. Note that $\mathbf{rank}(\mathbf{U})\leq K$. Hence, we have $N=\mathbf{rank}(\mathbf{U})\leq K$.

APPENDIX C
PROOF OF LEMMA 3

The lemma can be proved by showing the proposed example solution of (a,b,c) satisfies conditions (24) and (25). According to (28)-(29), b and c are defined based on a. The lemma holds if a can be found, while $\forall z\in(-\infty,Z], a\geq 0$ satisfying $\arctan(z)\geq -az^2+(\frac{1}{z_0^2+1}+2az_0)z+\arctan(z_0)+az_0^2-bz_0$.

According to (26), $a\geq 0$. In the following, we further discuss the following two cases, i.e., $0\leq a\leq\frac{1}{2(Z-z_0)(z_0^2+1)}$ and $a>\frac{1}{2(Z-z_0)(z_0^2+1)}$. In fact, when $a\leq\frac{1}{2(Z-z_0)(z_0^2+1)}$, it is easy to show that (24) and (25) hold. The main focus is on the case of $a>\frac{1}{2(Z-z_0)(z_0^2+1)}$, which corresponds $\frac{b}{2a}<Z$, i.e., the inequality (24) does not hold (at least it does not hold at point $z=\frac{b}{2a}$). According to (27), a should be adjusted. We introduce $\theta(z)=\arctan(z)+az^2-bz-c>0$ to guaranteeing the inequality (24). We can quickly have first derivative $\theta'(z)=(z-z_0)\big(2az^2-\frac{1}{z_0^2+1}z+2a-\frac{z_0}{z_0^2+1}\big)$. Clearly, $\theta(z_0)=0$ is guaranteed by the definition of b and c in (28)-(29). Hence, $\theta(z)\geq 0$ holds if we can find a satisfying the following three conditions: i. $\theta'(z)<0$ when $z<z_0$; ii. $\theta'(z)=0$ when $z=z_0$; iii. $\theta'(z)>0$ when $z>z_0$. These conditions further require $(2az^2-\frac{1}{z_0^2+1}z+2a-\frac{z_0}{z_0^2+1})\geq 0$, $\forall z\in(-\infty,Z]$, which is guaranteed in (27) as the following relationship holds

$$\begin{aligned}
&2az^2-\frac{1}{z_0^2+1}z+2a-\frac{z_0}{z_0^2+1}\geq 0\\
\overset{a\geq 0}{\Leftrightarrow}\ &z^2-\frac{1}{(z_0^2+1)\,2a}z+1-\frac{z_0}{(z_0^2+1)\,2a}\geq 0\\
\Leftrightarrow\ &\Big(z-\frac{1}{(z_0^2+1)\,4a}\Big)^2+1-\frac{z_0}{(z_0^2+1)\,2a}-\frac{1}{(z_0^2+1)^2 16a^2}\geq 0\\
\Leftarrow\ &16(z_0^2+1)^2a^2-8z_0(z_0^2+1)a-1\geq 0.
\end{aligned}$$

To sum up, with definitions of a,b,c in (26)-(29), conditions (24) and (25) are guaranteed.

REFERENCES

[1] Y. Zeng, R. Zhang, and T. J. Lim, "Wireless communications with unmanned aerial vehicles: Opportunities and challenges," *IEEE Commun. Mag.*, vol. 54, no. 5, pp. 36–42, May 2016.

[2] M. Mozaffari, W. Saad, M. Bennis, and M. Debbah, "Efficient deployment of multiple unmanned aerial vehicles for optimal wireless coverage," *IEEE Commun. Lett.*, vol. 20, no. 8, pp. 1647–50, Aug. 2016.

[3] L. Gupta, R. Jain, and G. Vaszkun, "Survey of important issues in UAV communication networks," *IEEE Communications Surveys & Tuts.*, vol. 18, no. 2, pp. 1123–52, Second Quarter 2016.

[4] A. Al-Hourani, S. Kandeepan, and S. Lardner, "Optimal LAP altitude for maximum coverage," *IEEE Wireless Commun. Lett.*, vol. 3, no. 6, pp. 569–72, Dec. 2014.

[5] M. Alzenad, A. El-Keyi, and H. Yanikomeroglu, "3-D placement of an unmanned aerial vehicle base station for maximum coverage of users with different QoS requirements," *IEEE Wireless Commun. Lett.*, vol. 7, no. 1, pp. 38–41, Feb. 2018.

[6] J. Lyu, Y. Zeng, R. Zhang, and T. J. Lim, "Placement optimization of UAV-mounted mobile base stations," *IEEE Commun. Lett.*, vol. 21, no. 3, pp. 604–07, Mar. 2017.

[7] Q. Wu, Y. Zeng, and R. Zhang, "Joint trajectory and communication design for multi-UAV enabled wireless networks," *IEEE Trans. Wireless Commun.*, vol. 17, no. 3, pp. 2109–21, Mar. 2018.

[8] M. Mozaffari, W. Saad, M. Bennis, and M. Debbah, "Unmanned aerial vehicle with underlaid device-to-device communications: Performance and tradeoffs," *IEEE Trans. Wireless Commun.*, vol. 15, no. 6, pp. 3949–63, Jun. 2016.

[9] R. Fan, J. Cui, S. Jin, K. Yang, and J. An, "Optimal node placement and resource allocation for UAV relaying network," *IEEE Wireless Commun. Lett.*, vol. 22, no. 4, pp. 808–11, Apr. 2018.

[10] Y. Zeng, R. Zhang, and T. J. Lim, "Throughput maximization for UAV-enabled mobile relaying systems," *IEEE Trans. Commun.*, vol. 64, no. 12, pp. 4983–96, Dec. 2016.

[11] V. Sharma, M. Bennis, and R. Kumar, "UAV-assisted heterogeneous networks for capacity enhancement," *IEEE Commun. Lett.*, vol. 20, no. 6, pp. 1207-10, Jun. 2016.

[12] C. Zhan, Y. Zeng, and R. Zhang, "Energy-efficient data collection in UAV-enabled wireless sensor network," *IEEE Wireless Commun. Lett.*, vol. 7, no. 3, pp. 328–31, Jun. 2018.

[13] F. Cheng, S. Zhang, Z. Li, Y. Chen, N. Zhao, F. R. Yu, and V. C. M. Leung, "UAV trajectory optimization for data offloading at the edge of multiple cells," *IEEE Trans. Veh. Tech.*, vol. 67, no. 7, pp. 6732–36, Jul. 2018.

[14] Q. Wu, J. Xu, and R. Zhang, "Capacity characterization of UAV-enabled two-user broadcast channel," *IEEE J. Sel. Areas Commun.*, vol. 36, no. 9, pp. 1955-71, Sept. 2018.

[15] L. Xie, J. Xu, and R. Zhang, "Throughput maximization for UAV-enabled wireless powered communication networks," *IEEE Internet Things J.*. Early Access, Oct. 2018.

[16] J. Xu, Y. Zeng, and R. Zhang, "UAV-enabled wireless power transfer: Trajectory design and energy region characterization," in *Proc. IEEE Globecom Workshops*, Singapore, 2017, pp. 1-7.

[17] J. Xu, Y. Zeng, and R. Zhang, "UAV-enabled wireless power transfer: Trajectory design and energy optimization," *IEEE Trans. Wireless Commun.*, vol. 17, no. 8, pp. 5092–06, Aug. 2018.

[18] F. Wang, J. Xu, X. Wang, and S. Cui, "Joint offloading and computing optimization in wireless powered mobile-edge computing systems," *IEEE Trans. Wireless Commun.*, vol. 17, no. 3, pp. 1784–97, Mar. 2018.

[19] F. Zhou, Y. Wu, R. Q. Hu, and Y. Qian, "Computation rate maximization in UAV-enabled wireless powered mobile-edge computing systems," *IEEE J. Sel. Areas Commun.*, Early Access, Aug. 2018.

[20] S. Zhang, Y. Zeng and R. Zhang, "Cellular-enabled UAV communication: trajectory optimization under connectivity constraint," *IEEE ICC 2018*, Kansas City, MO, 2018, pp. 1-6.

[21] S. Zhang, Y. Zeng, and R. Zhang, "Cellular-enabled UAV communication: A connectivity-constrained trajectory optimization perspective," *IEEE Trans. Commun.*, Early Access.

[22] H. Ju and R. Zhang, "Optimal resource allocation in full-duplex wireless powered communication network," *IEEE Trans. Commun.*, vol. 62, no. 10, pp. 3528–3540, Oct. 2014.

[23] S. Bi, C. K. Ho, and R. Zhang, "Wireless powered communication: Opportunities and challenges," *IEEE Commun. Mag.*, vol. 53, no. 4, pp. 117–25, Apr. 2015.

[24] X. Lu, P. Wang, D. Niyato, D. I. Kim, and Z. Han, "Wireless networks with RF energy harvesting: A contemporary survey," *IEEE Commun. Surveys & Tuts.*, vol. 17, no. 2, pp. 757–89, Second Quarter 2015.

[25] Arnold, Denise; Arnold, Graham (1993). *Four unit mathematics*. Hodder Arnold H&S. p. 242. ISBN 978-0-340-54335-1.

[26] S. Boyd. *EE364b Convex Optimization II, Course Notes*, accessed on Jun. 29, 2017. [Online]. Available: http://www.stanford.edu/class/ee364b/

[27] Bubeck, Sébastien. *Convex Optimization: Algorithms and Complexity*. Foundations & Trends in Machine Learning, 2014, 8(3-4):231-357. Available: https://arxiv.org/pdf/1405.4980v2.pdf

[28] R. Hunger, "Floating point operations in matrix-vector calculus," Munich University of Technology, TUM-LNS-TR-05-05, 2005.

[29] B. Clerckx, R. Zhang, R. Schober, D. W. K. Ng, D. I. Kim, and H. V. Poor, "Fundamentals of wireless information and power transfer: From RF energy harvester models to signal and system designs," [Online] Available: https://arxiv.org/abs/1803.07123

[30] W. Yu and R. Lui, "Dual methods for nonconvex spectrum optimization of multicarrier systems," *IEEE Trans. Commun.*, vol. 54, no. 7, pp. 1310–22, Jul. 2006.

[31] S. Boyd and L. Vandenberghe, Convex Optimization. *Cambridge, U.K.*: Cambridge Univ. Press, 2004.

[32] Yundi Wu, Jie Xu, Ling Qiu, Rui Zhang, "Capacity of UAV-enabled multicast channel: joint trajectory design and power allocation," *IEEE ICC 2018*, Kansas City, MO, 2018, pp. 1-7.

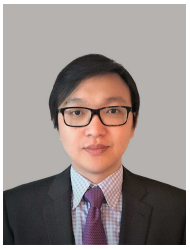

Yulin Hu (S11-M15-SM18) received his M.Sc.E.E. degree from USTC, China, in 2011. He successfully defended his dissertation of a joint Ph.D. program supervised by Prof. Anke Schmeink at RWTH Aachen University and Prof. James Gross at KTH Royal Institute of Technology in Dec. 2015 and received his Ph.D.E.E. degree (Hons.) from RWTH Aachen University where he was a postdoctoral Research Fellow since Jan. to Dec. in 2016. Since 2017, he works as a senior researcher and project lead in ISEK research group at RWTH Aachen University. From May to July in 2017, he was a visiting scholar with Prof. M. Cenk Gursoy in Syracuse University, USA. His research interests are in information theory, optimal design of wireless communication systems. He has been invited to contribute submissions to multiple conferences. He was a recipient of the IFIP/IEEE Wireless Days Student Travel Awards in 2012. He received the Best Paper Awards at IEEE ISWCS 2017 and IEEE PIMRC 2017, respectively. He served as a TPC member for many conferences and was an organizer of a special session in IEEE ISWCS 2018. He is currently serving as an editor for Physical Communication (Elsevier), an editor for EURASIP Journal on Wireless Communications and Networking and the lead editor of the Urllc-LoPIoT spacial issue in Physical Communication.

Xiaopeng Yuan received the B.Sc. degree in automation (control theory and control engineering) from Beijing University of Aeronautics & Astronautics, Beijing, China, in 2016. He is currently studying toward the M.Sc. degree in electrical engineering, information technology and computer engineering in RWTH Aachen University, and is expected to graduate in 2019. His research interests are in UAV trajectory design, information theory and optimization technology.

Jie Xu (S12-M13) received the B.E. and Ph.D. degrees from the University of Science and Technology of China in 2007 and 2012, respectively. From 2012 to 2014, he was a Research Fellow with the Department of Electrical and Computer Engineering, National University of Singapore. From 2015 to 2016, he was a Post-Doctoral Research Fellow with the Engineering Systems and Design Pillar, Singapore University of Technology and Design. He is currently a Professor with the School of Information Engineering, Guangdong University of Technology, China. His research interests include energy efficiency and energy harvesting in wireless communications, wireless information and power transfer, UAV communications, and mobile edge computing and learning. He was a recipient of the 2017 IEEE Signal Processing Society Young Author Best Paper Award, the 2018 IEEE Wireless Communications Letters Top Editor Award, the 2017 IEEE Access Outstanding Associate Editor, the 2015, 2017, and 2018 IEEE Transactions on Communications Exemplary Reviewer, the 2015 IEEE Transactions on Vehicular Technology Top Reviewer, and the 2014 IEEE Communications Letters Exemplary Reviewer. He is the Symposium Co-chair for IEEE Globecom 2019 Wireless Communications Symposium, the Workshop Co-Chair for ICC 2018 and ICC 2019 Workshop on UAV Communications, and the Tutorial Co-chair for IEEE/CIC ICCC 2019. He serves as an Editor of the IEEE Wireless Communications Letters and the Journal of Communications and Information Networks, an Associate Editor of the IEEE Access, and a Guest Editor of the IEEE Wireless Communications.

Anke Schmeink (M11-SM18) received the Diploma degree in mathematics with a minor in medicine and the Ph.D. degree in electrical engineering and information technology from RWTH Aachen University, Germany, in 2002 and 2006, respectively. She worked as a research scientist for Philips Research before joining RWTH Aachen University in 2008 where she is an associate professor since 2012. She spent several research visits with the University of Melbourne, and with the University of York. Anke Schmeink is a member of the Young Academy at the North Rhine-Westphalia Academy of Science. Her research interests are in information theory, systematic design of communication systems and bioinspired signal processing.